Comparison of Power Deposition by In-Phase 433 MHz and Phase-Modulated 915 MHz Interstitial Antenna Array Hyperthermia Systems

B. STUART TREMBLY, MEMBER, IEEE, ANDREW H. WILSON, JOHN M. HAVARD, KYRIACOS SABATAKAKIS, AND JOHN W. STROHBEHN, SENIOR MEMBER, IEEE

Abstract—**The interstitial microwave antenna array hyperthermia (IMAAH) system produces a pattern of specific absorption rate (*SAR*) that is nonuniform within a 2 cm square array when driven in phase at 915 MHz. Phase modulation makes the time-averaged *SAR* pattern significantly more uniform in planes perpendicular to the antennas. To drive antennas in phase at 433 MHz similarly improves *SAR* uniformity when the antennas are of resonance length.**

I. INTRODUCTION

IN HYPERTHERMIC treatment of cancer, the tumor temperature is raised above 42°C for about one hour. This subtle heating kills cells and potentiates the effect of radiation therapy [1]. While a final conclusion about efficacy is not yet possible, many biomedical engineers are working to solve the problem of delivering heat to a tumor in a controllable fashion [2].

One system developed and used in the clinic by the Dartmouth hyperthermia group is the interstitial microwave antenna array hyperthermia (IMAAH) system. This system heats a tumor through absorption of microwave energy radiated from an array of antennas implanted directly into the tumor. The antennas are linear dipoles made from flexible coaxial cable of 1.0 mm or 1.6 mm OD. They are inserted in the tumor through brachytherapy catheters, which are 2 mm OD nylon tubes used for implantation of iridium "seeds" for radiation therapy. This allows the clinician to combine hyperthermia and radiation therapy easily.

In this work we will consider an array of parallel antennas forming a square of 2 cm side length. We will refer to this square as the array boundary; in a treatment it would correspond roughly to the tumor boundary. We will display *SAR* and temperature data in two planes perpendicular to the antennas: the junction plane and the plane $z = 1.5$ cm (see Fig. 1). We drive the antennas at 915 MHz, and apply approximately 10 W per antenna. A feedback system controls the power to each antenna so as to keep local temperature constant, as measured by a fiber-optic microwave-immune temperature sensor inside each catheter. Presently, to maintain symmetry we drive the antennas in phase. Our system is described in [3] and [4]. The interstitial systems of other groups are described in [5]–[10].

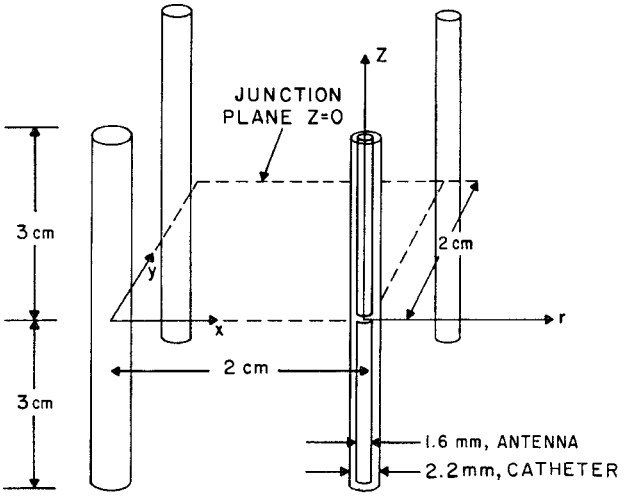

Fig. 1. The square array of four linear dipoles. The antenna junction plane and the x, y, r, and z directions are indicated.

With in-phase driving at 915 MHz, the pattern of specific absorption rate (*SAR*, W/kg) within the array boundary is characteristically nonuniform, since the array dimensions are comparable to a wavelength in tissue; thus, phase coherence effects are strong. Consequently, the physician cannot deliver a constant and well-defined thermal dose to the tumor. We have shown through theoretical calculation and through experiment that the point within the array at which the electric fields from all antennas add without cancellation can be moved about the array by delaying the driving phases of some antennas. This creates a local maximum of *SAR* at a known location [11].

In this paper we verify through experiment the improvement in time-averaged *SAR* uniformity obtained by focusing the maximum *SAR* in succession at four different points in the junction plane within the array boundary. We

Manuscript received June 29, 1987; revised November 16, 1987. This work was supported in part by the National Science Foundation under Grant ECS-8352580.

The authors are with the Thayer School of Engineering, Dartmouth College, Hanover, NH 03755.

IEEE Log Number 8819968.

0018-9480/88/0500-0908$01.00 ©1988 IEEE

will refer to this as phase modulation. We expand this investigation to show that the same behavior obtains in other transverse planes, and to compare these *SAR* patterns to the relatively uniform ones obtained at 433 MHz without phase modulation. We discuss the practical limitations of 433 MHz antennas. We also compare steady-state temperature distributions in tissue phantom at 915 MHz with and without phase modulation and at 433 MHz with in-phase driving. We do not present phantom temperatures as representative of those in tissue, but instead as a way to investigate the extreme case of zero blood flow.

II. Methods

The IMAAH antennas satisfy the theoretical requirements for calculation of the electric field by the one-dimensional numerical integration given in [12]. To estimate the electric field very close to the catheter we have used cubic spline interpolation between field values inside the catheter, where an accurate expression exists, and several catheter radii outside it, where the expression in [12] is accurate. This procedure is illustrated in [9, fig. 3]. Note a single cubic spline curve is fit to all of these computed field values; this yields a maximum field outside the insulation, and there is no discontinuity in the slope of the field. Casey and Bansal have shown by a more accurate numerical integration over two dimensions that this procedure overestimates the field just outside the catheter [14]. Their procedure allows a discontinuity in the slope at the insulator surface. In this paper we have used the simpler one-dimensional integration for convenience and because it gives a conservative prediction with respect to *SAR* uniformity. The resulting overprediction of the field close to the antenna is discussed below with reference to experimental results. *SAR* values calculated by our method a few mm from the antenna are accurate.

We measure the IMAAH system *SAR* pattern in Guy tissue phantom [15] by computing the initial rate of temperature rise in the instant after application of microwave power. To compute this, we measure temperature every five seconds for one minute, fit a single quadratic to these data points, and evaluate its initial slope. These measurements are made under computer control at points forming a 2×5 mm or 2×10 mm grid in a plane of the array perpendicular to the antennas. The computer converts the resulting matrix of discrete *SAR* values to lines of constant *SAR* through 2-D linear interpolation between points. This is how we display our *SAR* data in the figures below. We normalize our data by setting the maximum *SAR* to one. More details are given in [3].

The phase delays are provided by a solid-state phase shifter (Anghel Labs, Fairfield, NJ 07006) in line with each antenna. The phase shifter works in increments of 22.5° and is controlled by a four-bit signal from a microcomputer. The feedlines to all antennas have equal length to ensure they introduce no phase differences. Fig. 2(a) illustrates the focusing effect obtained with a phase delay at two antennas (cf. [7, fig. 4]). Fig. 2(b) illustrates successive focusing at four spots within the array obtained with phase modulation. The phase modulation is defined by the timing diagrams in Fig. 2(c). This cycle repeats every one second; this is much less than the one minute period of temperature measurement for *SAR* calculation. Therefore, successive focusing introduces insignificant error in the time-average *SAR* measurement.

In the steady-state temperature experiments, measurements were made with fiber-optic microwave-immune probes (Thermosentry 1200, Clini-Therm Corp., Dallas, TX) at nine points within the array: array center, each antenna, and each side midpoint. Each probe lay within a catheter strung through the plexiglass container before the tissue phantom was poured. In the first experiment, all antennas were driven in phase; this focused power in the array center. In the second experiment, power was focused between adjacent pairs of antennas by delaying the phase of those two antennas by 90° for 0.25 s at a time. Since this dwell time is much shorter than the thermal time constant of the phantom (about 6 min [4]), power is effectively focused at all four points simultaneously. In the third experiment, the phantom was heated by an array of resonant antennas driven in phase at 433 MHz.

The initial temperature in the phantom was relatively uniform, but was higher in the second experiment due to the heating in the first. To compare results, all temperatures $T(x, y)$ were normalized by subtracting the constant initial temperature T_0, then dividing by the highest temperature observed, T_M. This yields a normalized temperature $T'(x, y)$, which satisfies the steady-state bio-heat transfer equation with only a scale change in the *SAR* term, $P(x, y)$. The spatial variation of these normalized temperatures is of interest, not the absolute temperatures themselves. The interpretation of phantom temperatures is described in Section IV.

III. Results

In the *SAR* results below we show lines of constant *SAR* in one plane of the 2 cm square array shown in Fig. 1. The maximum *SAR* is normalized to 100 percent. The increment between iso-*SAR* lines is 10 percent or 25 percent of maximum, as specified. In all cases, the antenna has a 1.6 mm OD, and the catheter has 1.8 mm ID and 2.2 mm OD. The catheters' relative permittivity is 1.8, and the tissue has the electrical properties of muscle (relative permittivity = 51 at 915 MHz, = 54 at 433 MHz; conductivity = 1.3 S/m at 915 MHz, = 1.2 S/m at 433 MHz). In theoretical calculations, these numbers are entered into the computer program; in experiments, the tissue phantom constituents give the correct electrical properties [15]. All antennas are symmetric dipoles. Except in one specified case (Fig. 7), all antennas have their resonance length, which is a function of the wavelength in the catheter and in the tissue [12] (see Table I). Except in one specified case (Fig. 5), the junction plane is shown. The antennas were driven with nominally equal power; in some experiments individual power adjustments of up to 25 percent were made to compensate for variations in radiation efficiency among antennas. (We have found since then that with

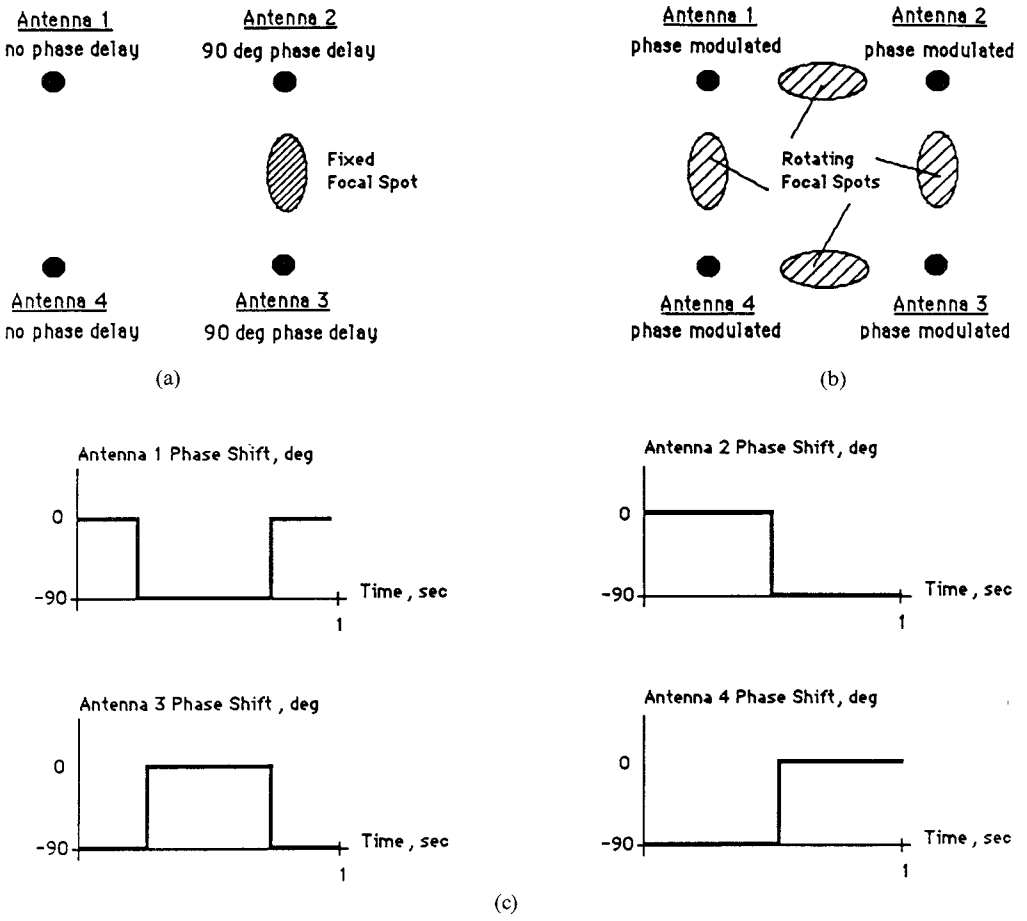

Fig. 2. (a) The junction plane of the array with a local *SAR* maximum between two antennas (focal spot) created by two fixed driving-phase delays of 90°. (b) The junction plane of the array with power focused in succession between pairs of antennas by phase modulation. (c) The phase modulation scheme as defined by the timing diagrams for the driving phases of all antennas. One period of the time cycle is shown.

TABLE I
THEORETICAL LENGTHS FOR RESONANT DIPOLES AND MONOPOLES AT 433 MHz AND 915 MHz

Frequency	Resonant Dipole	Resonant Monopole
915 MHz	5.4 cm	2.7 cm
433 MHz	10.2 cm	5.1 cm

careful construction of the antenna junction the radiated power varies only 5 percent among antennas in an array.) The small dots in the experimental results show the points of *SAR* measurement; these form a 2×5 mm or 2×10 mm rectangular grid. The antennas are shown as heavy dots.

Fig. 3 shows the measured *SAR* pattern in the junction plane of an array driven in phase at 915 MHz. This result is reproduced from an earlier paper for purposes of comparison [3]. Fig. 4(a) shows experimental results for antennas driven with phase modulation at 915 MHz. The increment between iso-*SAR* lines is 10 percent of maximum. The maximum *SAR* is at the upper right antenna, and *SAR* decreases to 40 percent of maximum at about 5 mm from the antenna. There is no local maximum at the array center. Within 60 percent of the array boundary, the *SAR* lies in the range 40–50 percent of maximum. In a repeat experiment the *SAR* at the array center differed by 1

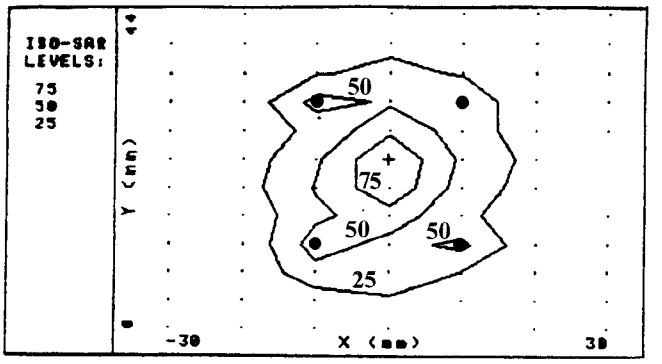

Fig. 3. Experimental lines of constant *SAR* in the junction plane of an array of resonant antennas driven in phase at 915 MHz. Measurements were made in muscle phantom. Antennas are shown by heavy dots, and points of *SAR* measurement are shown by light dots. Maximum *SAR* (location indicated by cross) is normalized to 100 percent, and the increment between lines is 25 percent of maximum. Reproduced from [3, fig. 8].

percent of maximum, and the average of array side-midpoint *SAR*'s differed by 1 percent of maximum. In both experiments the standard deviation of the four array side-midpoint measurements was about 5 percent of maximum; thus, there is greater variation among symmetric points in the array in a single experiment than between two different

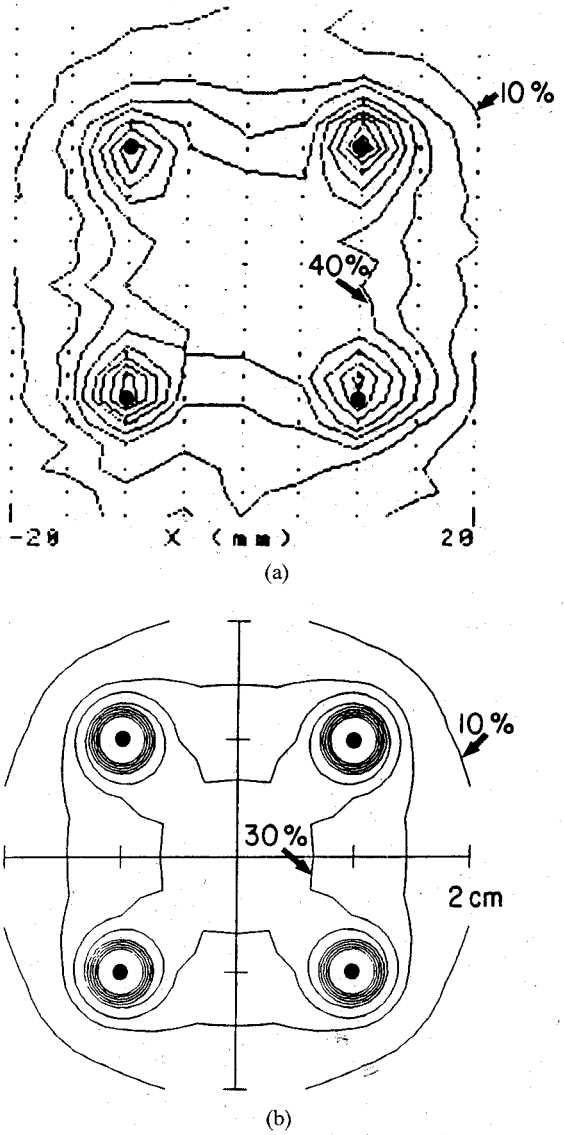

Fig. 4. (a) Experimental lines of constant *SAR* in the junction plane of an array of resonant antennas driven at 915 MHz with the phase modulation scheme defined in Fig. 2(c). Measurements were made in muscle phantom. Antennas are shown by heavy dots. Maximum *SAR* is normalized to 100 percent, and the increment between lines is 10 percent of maximum. (b) Theoretical result for same case.

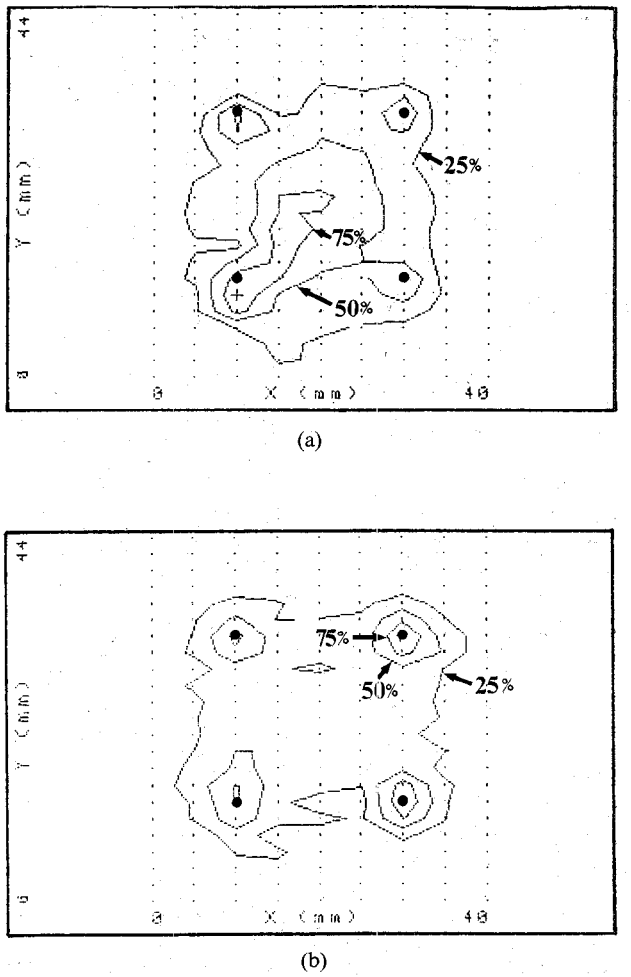

Fig. 5. (a) Experimental lines of constant *SAR* in the plane $z = 1.5$ cm of an array of resonant antennas driven at 915 MHz with equal phase. Antennas are shown by heavy dots. Maximum *SAR* is normalized to 100 percent, and the increment between lines is 25 percent of maximum. (b) Same as (a) with phase modulation defined by Fig. 2(c).

experiments. Fig. 4(b) shows the theoretical result for the same case. A steep *SAR* gradient is present at each antenna. The *SAR* within 60 percent of the array boundary lies in the range 30–40 percent of maximum.

Fig. 5(a) shows the measured *SAR* pattern in the plane $z = 1.5$ cm (Fig. 1). The frequency is 915 MHz with in-phase driving. The increment between iso-*SAR* lines is 25 percent of maximum for clarity. The maximum *SAR* occurs at the lower left antenna, and large *SAR* gradients are present at all antennas. An *SAR* peak occurs at the array center with a value greater than 75 percent of maximum; this iso-*SAR* line joins the lower left antenna to the array center due to asymmetry in array radiation. As in other experiments, power here was adjusted to make temperature rises equal at each antenna in the junction plane; however, *SAR* was not equal at each antenna in the plane $z = 1.5$ cm. This may be due to varying eccentricity of an antenna within the catheter lumen, which causes more energy to radiate from the side with smallest air gap [16].

Fig. 5(b) shows the time-averaged *SAR* pattern measured in the same plane with phase modulation. The maximum *SAR* occurs at an antenna, and large *SAR* gradients are present at all antennas. An *SAR* peak is not present at the array center; throughout 75 percent of the array boundary *SAR* is between 25 percent to 50 percent of maximum.

Fig. 6(a) shows the experimental *SAR* pattern in the junction plane of an array of resonant antennas driven in-phase at 433 MHz (half-length, defined as distance from driving point to either tip of dipole, equals 5 cm; see Table I). The increment between iso-*SAR* lines is 25 percent of maximum. (Since the 40 percent and 60 percent lines do not vary between Figs. 6 and 7, the coarser 25 percent increment is used for clarity.) The maximum *SAR* occurs at an antenna. The *SAR* at the array center is about 50 percent of maximum, and there is no sharply focused local *SAR* maximum there. The *SAR* pattern is asymmetric. Excluding the region within a few mm of each antenna, the

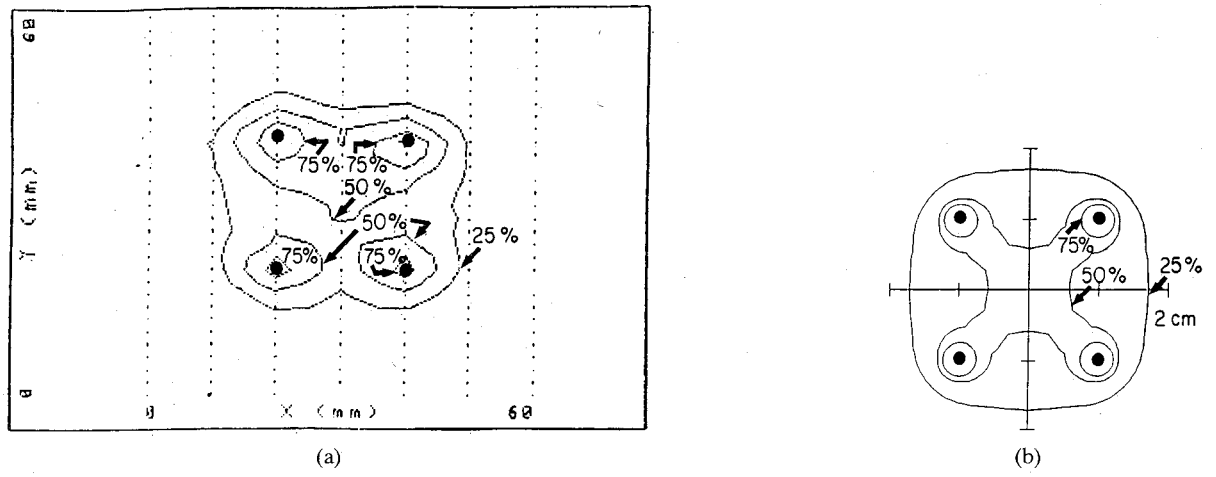

(a) (b)

Fig. 6. (a) Experimental lines of constant *SAR* in the junction plane of an array of resonant antennas driven at 433 MHz with equal phase. Antennas are shown by heavy dots. Maximum *SAR* is normalized to 100 percent, and the increment between lines is 25 percent of maximum. (b) Theoretical result for same case.

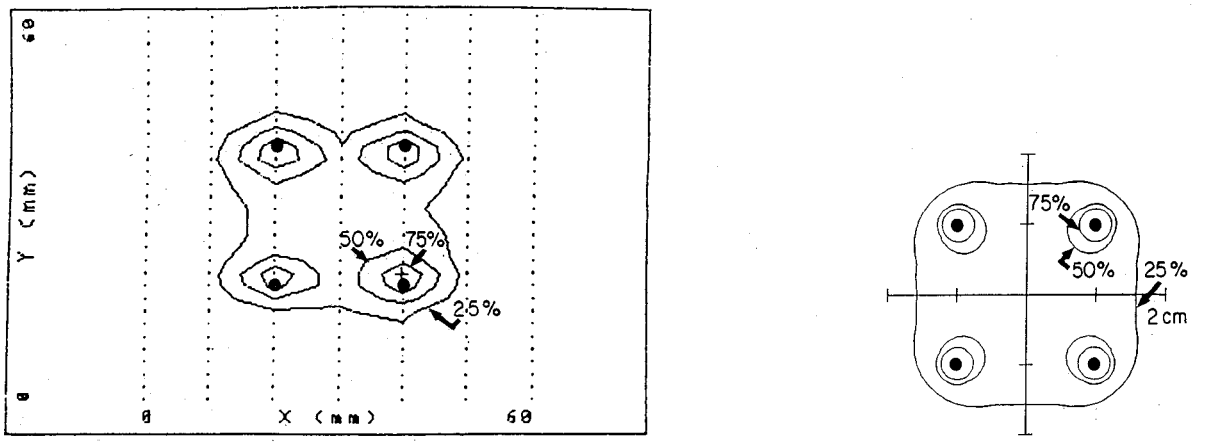

(a) (b)

Fig. 7. (a) Experimental lines of constant *SAR* in the junction of an array of subresonant antennas driven at 433 MHz with equal phase. Antennas are shown by heavy dots. Maximum *SAR* is normalized to 100 percent, and the increment between lines is 25 percent of maximum. (b) Theoretical result for same case.

SAR varies by less than 25 percent of maximum within the array boundary.

Fig. 6(b) shows the theoretical *SAR* pattern for the same case. The array center *SAR* is 50 percent of maximum, and the pattern is very similar to the experimental result. The *SAR* pattern is symmetric, since all antennas radiate the same power in the calculation.

Fig. 7(a) shows the experimental *SAR* pattern in the junction plane of an array of subresonant antennas (half-length equals 4 cm) driven in phase at 433 MHz. The *SAR* at the array center is less than 50 percent of maximum; a 50 percent iso-*SAR* line encloses each antenna separately. Fig. 7(b) shows the theoretical *SAR* pattern for the same case. As in experiment, *SAR* drops below 50 percent of maximum at points more than a few mm from each antenna.

Fig. 8(a) shows steady-state temperatures in muscle tissue phantom in the junction plane. The antennas are driven in phase at 915 MHz. The maximum temperature is at the array center, and the rise above the initial value is normalized to unity. The temperature distribution is not symmetric due to differences in radiation efficiency among antennas. The average normalized antenna temperature is 0.57; the average array side-midpoint temperature is 0.77. The greatest variation within the array boundary is 45 percent of maximum. This temperature distribution depends directly on the *SAR* distribution; since the *SAR* distributions varied only 1 percent between runs, we would expect the repeatability of temperature measurements to be similar.

Fig. 8(b) shows steady-state temperatures with phase modulation at 915 MHz. The temperature distribution is not symmetric. The average normalized antenna temperature is 0.79, and the average side midpoint temperature is 0.89. The greatest variation within the array boundary is 24 percent of maximum. In the plane $z=1.5$ cm (results not shown) phase modulation reduced the variation in normalized temperature within the array boundary from

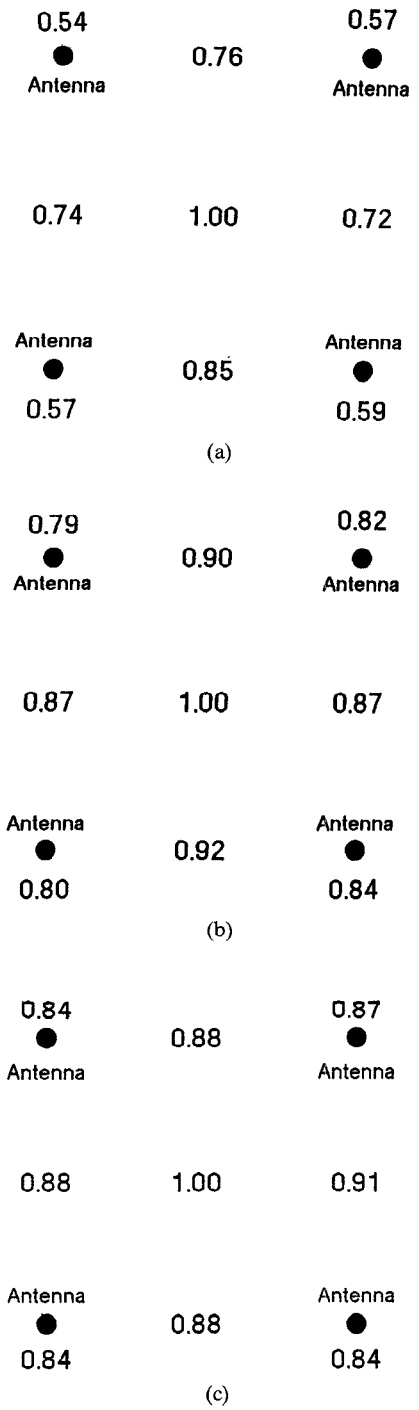

Fig. 8. (a) Experimental normalized steady-state temperatures in muscle phantom at discrete points in the junction plane of an array of resonant antennas driven at 915 MHz with equal phase. Antennas are shown by heavy dots. Maximum temperature is normalized to 1.00. (b) Same as (a) but with the phase modulation scheme defined in Fig. 3(c). (c) Same as (a) but with antennas driven at 433 MHz with equal phase.

34 percent to 24 percent of maximum; in the plane $z = 4$ cm (beyond antenna tip) phase modulation reduced the same variation from 47 percent to 34 percent of maximum.

Fig. 8(c) shows steady-state temperatures at 433 MHz with in-phase driving. The temperature distribution is not symmetric. The average normalized antenna temperature is 0.85, and the average side midpoint temperature is 0.89. The greatest variation within the array boundary is 15 percent of maximum.

IV. Discussion

Fig. 3, reproduced from [3], shows that with in-phase driving at 915 MHz, the maximum *SAR* occurs at the array center. The *SAR* at the antennas and the edge of the array boundary is about 50 percent of maximum. This *SAR* distribution is roughly the reverse of the ideal *SAR* distribution derived by Ocheltree *et al.* for simple geometries with spatially uniform blood flow [17]. Those authors conclude that the *SAR* must be greatest at the tumor margin (a spatial impulse function in the limit) and must have a smaller, constant value everywhere else within the tumor.

We have shown in this paper how the *SAR* peak at the array center can be eliminated, leaving a relatively constant value within the array boundary, except for peaks at the antennas. This is accomplished by a phase delay of two antennas, which shifts the local *SAR* maximum from the array center to a point on the array side-midpoint, as in [11, Fig. 4]; the measured magnitude of this new local maximum is 60 percent of maximum (50 percent, theoretical) [11]. When this local maximum is rotated rapidly among the four array side-midpoints, the time-averaged *SAR* becomes more uniform. Within 90 percent of the array boundary *SAR* is in the range 40–50 percent of maximum. Maximum *SAR* occurs at the antennas. This is a significant improvement over in-phase driving, as will be discussed below.

We have tried phase modulation with delays other than 90°; these gave smaller time-averaged *SAR* at the array center. We have tried a set of 0, 45, 90, 112.5° delays (eight-way symmetry); this yielded an *SAR* of 80 percent of maximum at the array center, but uniformity was poorer than in Fig. 4(b). Due to attenuation it is not possible to focus significant power outside the array boundary with any values of phase delays. Thus, the failure of a phase shifter will not cause large amounts of power to be focused in normal tissue.

In Fig. 4 theory predicts a smaller time-averaged value than experiment at the array center (30 percent versus, 40 percent of maximum). This underprediction can be avoided by using linear interpolation between the known electric field value at the catheter surface and the known point several mm from the surface calculated with our 1-D numerical integration technique. This permits a discontinuity in the slope of the field at the catheter surface, as discussed in [14].

The local *SAR* maximum at each antenna cannot be reduced by phase modulation, because it is associated with attenuation. However, thermal conduction will smooth these peaks if blood perfusion does not dominate tumor heat transfer; tissue thermal properties and array geometry determine what blood flow value is sufficiently low for this effect [18]. As discussed below, maximum power deposition at the array corners can be desirable in producing more uniform temperature with low blood perfusion. How-

ever, high blood perfusion will yield a temperature distribution with a shape similar to the *SAR* distribution, and this is nonuniform [18]. Convective cooling within each antenna could be used to reduce the local tissue temperature [19], [20]. We have found that air cooling (6 L/min at 20°C) of a single antenna heating a dog kidney will reduce the temperature adjacent to the antenna by 3°C while reducing the temperature 5 mm away by only 0.5°C [unpublished results]. Therefore, phase modulation combined with air cooling may improve temperature uniformity in the presence of high blood flow. A paper on air cooling is in preparation.

The same effects of phase modulation are seen in the plane $z = 1.5$ cm as in the junction plane. Fig. 5(a) shows a large *SAR* value at the array center with in-phase driving at 915 MHz; as discussed above, this is undesirable. In this plane the absolute *SAR* is about 75 percent of that in the junction plane; consequently, the signal-to-noise ratio is poorer, especially for the 25 percent line. Furthermore, the computer uses 2-D linear interpolation to draw the iso-*SAR* lines between the discrete data points. Since these points form a rectangular—not square—grid, a zigzag distortion results in some places. Nonetheless, the data reveal a distribution similar to that in the junction plane (Fig. 3) in spite of the noise and distortion. The overall asymmetry in Fig. 5(a) has been discussed above.

In Fig. 5(b) the time-averaged *SAR* with phase modulation shows an improvement in uniformity at points more than 5 mm away from the antennas; the *SAR* there is uniform within 25 percent of maximum. Thus, the same smoothing effect obtains as in the junction plane. This is to be expected, since the antenna current is a standing wave (the antenna can be modeled as an open-circuited transmission line) [12]; thus, the current at all points along the antenna has the same phase with respect to time variations. A driving phase difference for one antenna with respect to another will therefore have the same effect at all points along the antenna.

Fig. 6 shows the *SAR* pattern of a 433 MHz system is relatively uniform within the junction plane with in-phase driving. The array center *SAR* is above 50 percent of maximum for both theory and experiment, a slight improvement over the phase-modulated 915 MHz case, which yielded between 40 percent and 50 percent of maximum at the array center (Fig. 4(a)). A steep *SAR* gradient is present near each antenna. In the experimental result the 50 percent iso-*SAR* line is broken, since several central data points fell below this threshold. This asymmetry is due to a mismatch among antennas. We conclude that a 433 MHz *SAR* uniformity can be improved over that of the 915 MHz in-phase system without added phase-shifting components. In the case of high blood perfusion, conduction does not dominate heat transfer in the array. Since the temperature distribution is then similar to the *SAR* distribution, the antenna temperature could be too high if array center temperature were therapeutic. If so, the antenna temperature could be reduced by air cooling, as has been done in a 300 MHz system [20].

The resonant dipole is 10.2 cm long when driven at 433 MHz (Table 1); this is longer than many tumors. Thus, the antenna may heat normal tissue, or protrude from a superficial tumor, in which case the presence of air will cause a large impedance mismatch. Figs. 6 and 7 show that *SAR* uniformity is poorer when the dipole has a length less than resonant in that the region within the array boundary with *SAR* above 50 percent of maximum has been reduced from about 60 percent to about 20 percent in both theory and experiment. In these figures the antenna half-length was reduced by only 1.1 cm, from the resonance value of 5.1 cm to 4 cm. To reduce the half-length further to 3 cm (the resonance half-length at 915 MHz) would decrease array center *SAR* greatly with 433 MHz driving, since such a short antenna is very inefficient. We have shown this in a theoretical study of a 400 MHz 3 cm square array in which the array center *SAR* with antennas of 3 cm half-length was one fourth that with resonant antennas [13].

It would be possible to heat a tumor with short antennas if increased microwave power and air cooling were applied to raise the absolute power delivered to the array center without burning tissue near the antenna. However, there is a limit to this, since subresonant antennas do not have a purely real input impedance [12]; therefore, the reflected power will heat the feedline inside the patient to high temperatures. This could destroy the cable, burn the skin, or negate the effects of air cooling. A better solution would be to use a monopole of resonance length over a ground plane if the tumor were superficial. We have described a ground plane that will not interfere with the catheter in the clinic [21]. We have considered phase modulation at 433 MHz. However, phase delays do not change the *SAR* pattern dramatically at this frequency in a 2 cm array, since the array is smaller than a wavelength.

While the *SAR* distribution represents a steady-state temperature distribution in the extreme case of infinite blood blow, the steady-state temperature distribution in phantom represents the case of no blood flow. By investigating phase modulation for these two extremes, we have bracketed all other values of spatially uniform blood flow. If phase modulation improves uniformity for the bracketing cases, we can conclude uniformity is also improved for all intermediate cases. This is how phantom temperatures are useful; we do not assume that the temperature distribution in phantom predicts the temperature distribution in tissue.

In phantom, the large *SAR* near each antenna does not produce a local temperature maximum, because thermal conduction dominates. Since little power is deposited outside the array boundary, the antenna in its corner position is at the vertex of a 270° arc of unheated tissue. A large heat flux outward in this arc reduces the steady-state temperature at the antenna. For this reason, the array temperature is lowest at the antennas with or without phase modulation. However, phase modulation at 915 MHz improves significantly the temperature uniformity within the array boundary. The temperature distribution with 433 MHz in-phase driving is similar to the phase-

modulated 915 MHz case, as would be expected from their similar *SAR* patterns. Note that the asymmetry in temperature observed could be eliminated through dwell time modulation based on local temperature feedback. This could compensate for mismatches among antennas and, more importantly, could compensate for nonuniformities in tissue electrical and thermal properties. Power modulation could accomplish the same thing.

We have described improvements in uniformity in the plane perpendicular to the antennas. However, uniformity parallel to the antennas is poor [3]. New antenna geometries may improve this [22]–[25]. Such new designs could be combined with the techniques described here to improve uniformity in both directions.

V. Conclusions

At 915 MHz, suitable phase delays will focus power absorption away from the array center, where *SAR* is maximum with in-phase driving. By focusing in rapid succession at four symmetric points in the array (phase modulation), the time-averaged *SAR* becomes more uniform: the variation is 10 percent of maximum within 90 percent of the array boundary in the junction plane. By comparison, with in-phase driving the *SAR* varies by 50 percent of maximum within the array boundary. Phase modulation similarly improves *SAR* uniformity in planes other than the junction plane. Phase modulation improves temperature uniformity in tissue phantom simulating tissue with no blood perfusion. Antenna mismatches and tissue nonuniformity must be compensated for through feedback control to yield symmetric temperature distributions.

Driving resonant antennas in phase at 433 MHz yields an *SAR* pattern similar to the phase-modulated 915 MHz pattern. Using antennas shorter than resonance length yields reduced power deposition in the array center and thus poorer *SAR* uniformity.

References

[1] G. M. Hahn, *Hyperthermia and Cancer*. New York: Plenum Press, 1982, pp. 1–285.

[2] J. W. Strohbehn and E. B. Douple, "Hyperthermia and cancer therapy: A review of biomedical engineering contributions and challenges," *IEEE Trans. Biomed. Eng.*, vol. BME-31, pp. 779–787, 1984.

[3] T. Z. Wong, J. W. Strohbehn, K. M. Jones, J. M. Mechling, B. S. Trembly, "SAR patterns from an interstitial microwave antenna-array hyperthermia system," *IEEE Trans. Microwave Theory Tech.*, vol. MTT-34, pp. 560–568, May 1986.

[4] K. F. Smith, "Computer implementation of an interstitial microwave antenna array hyperthermia system," Master of Engineering thesis, Thayer School of Engineering, Dartmouth College, Aug. 1983.

[5] G. M. Samaras, "Intracranial microwave hyperthermia: Heat induction and temperature control," *IEEE Trans. Biomed. Eng.*, vol. BME-31, pp. 63–69, Jan. 1984.

[6] P. F. Turner, "Invasive hyperthermia apparatus and method," U.S. Patent 4 448 198; 1984.

[7] L. S. Taylor, "Implantable radiators for cancer therapy by microwave hyperthermia," *Proc. IEEE*, vol. 6, pp. 142–149, Jan. 1980.

[8] B. E. Lyons, R. H. Britt, and J. W. Strohbehn, "Localized hyperthermia in the treatment of malignant brain tumors using an interstitial microwave antenna array," *IEEE Trans. Biomed. Eng.*, vol. BME-31, pp. 53–62, 1984.

[9] J. C. Lin and Y. J. Wang, "Interstitial microwave antennas for thermal therapy," *Int. J. Hyperthermia*, vol. 3, pp. 37–47, 1987.

[10] D. J. Lee, M. J. O'Neill, K. S. Lam, R. Rostock, and W. C. Lam, "A new design of microwave interstitial applicators for hyperthermia with improved treatment volume," *Int. J. Radiat. Oncology*, vol. 12, pp. 2003–2008, Nov. 1986.

[11] B. S. Trembly, A. H. Wilson, M. J. Sullivan, A. D. Stein, T. Z. Wong, and J. W. Strohbehn, "Control of the SAR pattern within an interstitial microwave antenna array through variation of antenna driving phase," *IEEE Trans. Microwave Theory Tech.*, vol. MTT-34, pp. 568–571, May 1986.

[12] R. W. P. King, B. S. Trembly, and J. W. Strohbehn, "The electromagnetic field of an insulated antenna in a conducting or dielectric medium," *IEEE Trans. Microwave Theory Tech.*, vol. MTT-31, pp. 574–583, July 1983.

[13] B. S. Trembly, "The effects of driving frequency and antenna length on power deposition within a microwave antenna array used for hyperthermia," *IEEE Trans. Biomed. Eng.*, vol. BME-32, pp. 152–157, Feb. 1985.

[14] J. P. Casey and R. Bansal, "The near field of an insulated dipole in a disspative dielectric medium," *IEEE Trans. Microwave Theory Tech.*, vol. MTT-34, pp. 459–463, Apr. 1986.

[15] A. W. Guy, "Analysis of electromagnetic fields induced in biological tissues by thermographic studies on phantom equivalent models," *IEEE Trans. Microwave Theory Tech.*, vol. MTT-19, pp. 205–214, Feb. 1971.

[16] T. T. Wu, L. C. Shen, and R. W. P. King, "The dipole antenna with eccentric coating in a relatively dense medium," *IEEE Trans. Antennas Propagat.*, vol. AP-22, pp. 57–62, Jan. 1975.

[17] K. B. Ocheltree and L. A. Frizzell, "Determination of power deposition patterns for localized hyperthermia: A steady-state analysis," *Int. J. Hyperthermia*, vol. 2, no. 3, pp. 269–279, 1987.

[18] J. W. Strohbehn, B. S. Trembly, E. B. Douple, "Blood flow effects on the temperature distributions from an invasive microwave antenna array used in cancer therapy," *IEEE Trans. Biomed. Eng.*, vol. BME-29, pp. 649–661, Sept. 1982.

[19] J. Scheiblich and O. Petrowicz, "Radiofrequency-induced hyperthermia in the prostate," *J. Microwave Power*, vol. 17, no. 3, pp. 203–209, 1984.

[20] H. I. Bicher, D. W. Moore, and R. W. Wolfstein, "A method for interstitial thermoradiotherapy," in *Proc. 4th Int. Symp. Hyperthermic Oncol.*, 1984, pp. 595–598.

[21] B. S. Trembly, J. W. Strohbehn, and R. W. P. King, "Practical embedded insulated antenna for hyperthermia," in *Proc. 10th Ann. Northeast Bioeng. Conf.*, 1982, pp. 105–108.

[22] D. Roos, "Analysis of the temperature distribution produced by an invasive microwave applicator for heat treatment of cancer," Rpt. no. 4, ISSN 0281-8914, Dept. of Appl. Elec. Phys., Chalmers Univ. of Tech., Göteborg, Sweden, 1984.

[23] P. F. Turner, "Interstitial EM applicator/temperature probes," in *Proc. 8th Ann. Conf. IEEE EMB Soc.*, 1986, pp. 1454–1457.

[24] Y. Wang and J. C. Lin, "A comparison of microwave interstitial antennas for hyperthermia," in *Proc. 8th Ann. Conf. IEEE EMB Soc.*, 1986, pp. 1463–1466.

[25] A. Wu, M. L. Watson, E. S. Sternick, R. J. Bielawa, and K. L. Carr, "Performance characteristics of a helical microwave interstitial antenna for local hyperthermia," *Med. Phys.*, vol. 14, no. 2, pp. 235–237, Mar. 1987.

✠

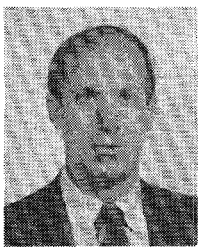

B. Stuart Trembly (M'83) received the B.S. degree from Yale University, New Haven, CT, in 1975, and the Ph.D. degree from Dartmouth College, Hanover, NH, in 1982.

He joined the faculty at the Thayer School of Engineering at Dartmouth College in 1982, where he is an Assistant Professor. His research interest is the application of electrical engineering to biomedical problems.

Dr. Trembly was the recipient of a Presidential Young Investigator Award in 1984.

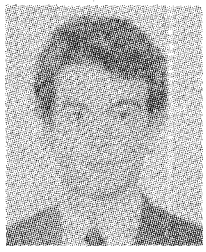

Andrew H. Wilson was born in Bulter, PA, on October 9, 1957. He received the B.A. degree from Harvard College in 1980, the M.B.A. degree from the Tuck School of Business Administration in 1985, and the M.E. degree from the Thayer School of Engineering, Dartmouth College, in 1986.

✠

John M. Havard was born in New Rochelle, NY, on December 11, 1960. He received the A.B. degree from Dartmouth College in 1983 and the M.E. degree from the Thayer School of Engineering, Dartmouth College, in 1987.

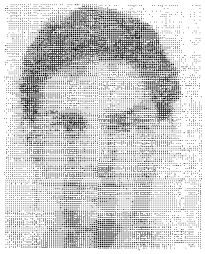

Kyriacos G. Sabatakakis was born in Athens, Greece, on March 18, 1965. He received the B.S. degree from Yale College in 1986 and the M.S. degree from the Thayer School of Engineering, Dartmouth College, in 1987.

✠

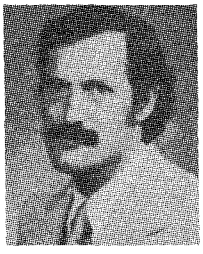

John W. Strohbehn (S'57–M'64–SM'81) received the B.S., M.S., and Ph.D. degrees in electrical engineering from Stanford University, Stanford, CA, in 1958, 1959, and 1964, respectively.

He joined the faculty at the Thayer School of Engineering, Dartmouth College, Hanover, NH, in 1963, where he currently holds the position of Professor of Engineering. His research efforts have been in the fields of radiophysics, including microwave and optical propagation through the atmosphere, and in biomedical engineering, including image processing tomography and the use of heat in the cure and control of cancer.

Dr. Strohbehn is a Fellow of the Optical Society of America and a member of the American Association for the Advancement of Science and of URSI Commission II. He was a National Academy Exchange Scientist to the Soviet Union in 1964. He served as an Associate Editor of the IEEE TRANSACTIONS ON ANTENNAS AND PROPAGATION from 1969 to 1971 and is currently Associate Editor of the IEEE TRANSACTIONS ON BIOMEDICAL ENGINEERING. Dr. Strohbehn was a Visiting Research Scientist at the Stanford University Medical School in 1981–1982.